HHS Public Access

Author manuscript

Cancer Res. Author manuscript; available in PMC 2020 May 15.

Published in final edited form as:

Cancer Res. 2019 May 15; 79(10): 2564–2579. doi:10.1158/0008-5472.CAN-18-2674.

Genome-wide interrogation of human cancers identifies EGLN1 dependency in clear cell ovarian cancers

Colles Price[1,2,3], **Stanley Gill**[1,2], **Zandra V. Ho**[1], **Shawn M. Davidson**[1,4], **Erin Merkel**[1], **James M. McFarland**[1], **Lisa Leung**[1], **Andrew Tang**[1], **Maria Kost-Alimova**[1], **Aviad Tsherniak**[1], **Oliver Jonas**[1,4], **Francisca Vazquez**[1,2], and **William C. Hahn**[1,2,3,5,#]

[1]Broad Institute of Harvard and MIT, 415 Main Street, Cambridge, MA, USA

[2]Department of Medical Oncology, Dana-Farber Cancer Institute, 450 Brookline Avenue, Boston, MA, USA

[3]Harvard Medical School, 25 Shattuck Street, Boston, MA, USA.

[4]Koch Institute for Integrative Cancer Research, Massachusetts Institute of Technology, Cambridge, Massachusetts, USA.

[5]Department of Medicine, Brigham and Women's Hospital, 75 Francis Street, Boston, MA, USA.

Abstract

We hypothesized that candidate dependencies for which there are small molecules that are either approved or in advanced development for a non-oncology indication may represent potential therapeutic targets. To test this hypothesis, we performed genome-scale loss-of-function screens in hundreds of cancer cell lines. We found that knockout of *EGLN1*, which encodes Prolyl Hydroxylase Domain-Containing Protein 2 (PHD2), reduced the proliferation of a subset of clear cell ovarian cancer cell lines *in vitro*. EGLN1-dependent cells exhibited sensitivity to the pan-EGLN inhibitor FG-4592. The response to FG-4592 was reversed by deletion of HIF1A, demonstrating that EGLN1 dependency was related to negative regulation of HIF1A. We also found that ovarian clear cell tumors susceptible to both genetic and pharmacological inhibition of EGLN1 required intact HIF1A. Collectively, these observations identify EGLN1 as a cancer target with therapeutic potential.

Introduction

The development of genome scale methods to interrogate the function of genes now provides a path to systematically identify genes that are essential for cell survival. Several studies using RNAi and more recently CRISPR-Cas9 to suppress or delete genes have identified cell essential genes in human cancer cell lines (1–8). Compared to similar experiments in yeast (9,10), these studies have identified a larger number of essential genes in human cells (7, 10–12).

[#]Corresponding author: william_hahn@dfci.harvard.edu.

We and others have used similar approaches to identify genes that are essential for subsets of cancer cell lines (7, 10–13). A number of screens involving a modest number of cell lines have identified several cancer dependencies related to oncogenic mutation (12) or genes that become required in the setting of loss of a paralog (11, 13). In recent work, we and others have expanded such efforts to hundreds of cancer cell lines and defined several types of dependencies that occur in subsets of cancers (2, 5, 7, 12, 13). Such efforts will eventually lead to a comprehensive map of cancer dependencies.

A direct downstream sensor of oxygen tension is the family of prolyl hydroxylases called EGLN (Egg-laying defective nine homolog). When oxygen is present EGLN, also known as hypoxia-inducible factor prolyl hydroxylase (HIF-PH) and prolyl hydroxylase domain-containing protein (PHD), hydroxylates HIF1 which results in a binding site for a ubiquitin ligase complex that includes VHL, leading to HIF1 degradation (14–17). This leads to HIF1 degradation by forming a binding site for a ubiquitin ligase complex that includes VHL (14–17). Among the three EGLN family members, EGLN1 is generally regarded as the primary HIF1 hydroxylase, while EGLN2 and EGLN3 regulate HIF1 under specific conditions (15–17). With decreased concentrations of oxygen, EGLN-mediated hydroxylation of HIF1 is reduced which leads to increased levels of HIF1 (17). When HIF1 is increased under low oxygen conditions, the α subunit heterodimerizes with the β subunit and translocates to the nucleus to activate genes that promote glucose uptake, glycolysis and decreases oxidative phosphorylation (17).

We initiated an effort to identify differential dependencies by interrogating the data derived from screening a large number of cell lines with genome scale RNAi and CRISPR-Cas9 libraries. From a list of nominated strong preferential dependencies, we identified EGLN1 as a dependency preferentially required for the viability of a subset of cancer cell lines.

Materials and Methods

Analysis of Dependency Data

We used gene dependency data from Project Achilles including data from the screening of 501 cancer cell lines by RNAi (~94k shRNAs, ~5 shRNAs/gene) and 436 cancer cell lines with CRISPR-Cas9 (~70k sgRNAs, ~4 sgRNAs/gene) (1–5). EGLN1 was originally identified as an interesting target to pursue using the DEMETER six sigma dependencies (2). Further analyses were performed using CERES CRISPR/Cas9 dependency data (7, 18–22) and DEMETER2 RNAi (20, 21). All significant findings are summarized in the supplemental tables.

Identifying features associated with EGLN1 dependency

We used multiple approaches to find relationships between EGLN1 dependency and mRNA expression, copy-number, mutation, or dependency data (see CCLE Omics Data section for details). To identify genes whose mutation was associated with EGLN1 dependency, we used two-sample t-tests to measure the mean-difference of dependency between mutant and WT cell lines for each gene and type of mutation (damaging or missense). Only mutations present in at least 5 cell lines were included in the analysis. To identify other continuous-

valued (expression, copy-number, dependency) features associated with EGLN1 dependency, we used the R package Limma. Linear model coefficients were used to assess the strength of association between each feature and EGLN1 dependency, P-values were determined using empirical-Bayes moderated t-statistics (analyzing each data type separately). Note that we also used this method to identify top dependencies associated with HIF1A expression in Supplementary Figure 1M.

CCLE Omics Data

We used the following CCLE (22) datasets available for download at https://depmap.org/portal/download/all/.

mRNA Expression: CCLE_DepMap_18Q2_RNAseq_RPKM_20180502.gct

Copy-number: public_18Q2_gene_cn_v2.csv

Damaging/Non-damaging Mutations: CCLE_DepMap_18Q2_maf_20180502.txt (genes are classified as having a “damaging mutation” if isDeleterious is “TRUE” for any of its mutations).

Identifying gene sets associated with EGLN1 dependency

Using the GenePattern software platform developed by the Broad Institute, we ran single-sample GSEA (ssGSEA) on ovarian mRNA expression to calculate the activity level of each HALLMARK gene set in each ovarian cell line (using the Hallmark collection from the Molecular Signatures Database. We then found gene sets whose ssGSEA values were associated with EGLN1 dependency using linear model analysis as mentioned above.

Lineage enrichment analysis

Using a one-sided Fisher’s exact test, we measured the positive enrichment of EGLN1-dependent lines in a given lineage compared to all other lineages. We defined CRISPR EGLN1-dependencies as cell lines with at least a 50% probability of being dependent, leveraging the CERES probabilities of dependency that were published alongside the CERES effect scores (19). Lineages represented by fewer than 5 lines were filtered out and false discovery rates were calculated to correct for multiple hypothesis testing.

Cell Culture Conditions

All cell lines were provided from stocks curated by the Cancer Dependency Map project at the Broad Institute and originally obtained from the Cancer Cell Line Encyclopedia (www.broadinstitute.org/ccle) unless otherwise indicated. All cell lines were fingerprinted using one of two genotyping platforms, Sequenom or Fluidigm. Mycoplasm testing was performed when cell lines were obtained from CCLE. Cell lines expressing pLX_311-cas9 were generated by the Project Achilles for use in the genome-wide pooled CRISPR screening data used to inform this project. ES2, OVTOKO, TOV112D, HEYA8, OVISE were cultured in RPMI-1640+10% FBS. OVK18 was cultured in MEM+10% FBS. COV434 was cultured in DMEM+10% FBS+2mM Glutamine. TOV21G was cultured in

MCDB105:Medium199 (1:1)+15% FBS. JHOC5 was cultured in DMEM:F12 (1:1)+10% FBS+0.1mM NEAA. All media were supplemented with penicillin-streptomycin.

Vectors and Constructs

All vectors and plasmids used for these experiments, where they were obtained and sequences for all sgRNAs designed are listed in Supplementary Table 1.

Arrayed Lentivirus Production

293T cells were seeded in 6 well plates at $1.5X10^6$ per well (2mL volume) 24 h pre-transfection. Transfection was performed using TransIT-LTI Transfection Reagent (Mirus). 8.25uL of LT1 was diluted in 75uL of Opti-Mem (Corning) for each well and incubated at room temperature for 5 min. The diluted LTI mixture was added to a mixture of 1250 ng PsPAX2, 250ng VSVG, and 1250 ng lentivector DNA suspended in Opti-MEM and incubated at room temperature for 20 – 30 minutes. The transfection mixture was then added to the plate of cells, spun at 1000g for 30 min, and incubated at standard cell culture conditions (37°C, 5% CO2) for 6 – 8 h. Media were then changed to high serum media (DMEM + 30% FBS) and incubated until harvest after 48–72 h. Virus was stored at −80°C until use in the experiments.

Immunoblots

Cells were infected with lentiviruses expressing sgRNAs targeting EGLN1 and selected with puromycin at a concentration of 4ug/mL for 48–72 h or until all uninfected cells were dead. Whole cell lysates were prepared using RIPA buffer (Sigma-Aldrich) supplemented with EDTA-free Protease Inhibitor Cocktail (Roche), 1mM Sodium Orthovanadate (NEB), and 5mM Sodium Fluoride (NEB). Protein levels were quantified using the Pierce BCA assay kit (Thermo Fisher Scientific). Protein lysates were run on 4–12% Bis-Tris Pre-Cast gels (Thermo Fisher Scientific) and proteins transferred to a PVDF membrane using the iBlot 2 system (Thermo Fisher Scientific). HIF1a levels were detected using a mouse monoclonal anti-HIF1a Antibody at 1:1000 dilution (BD Biosciences #610958) and a LICOR-compatible anti-mouse IR secondary antibody (LICOR #926–68020) at 1:5000 dilution. EGLN1 levels were detected using a rabbit monoclonal EGLN1 antibody (Cell Signaling #3293) at 1:1000 and a LICOR-compatible anti-rabbit IR secondary antibody (#926–32211) at 1:5000 dilution. VHL levels were detected using a rabbit monoclonal VHL antibody (Cell Signaling #685475) and a LICOR-compatible anti-rabbit IR secondary antibody. GAPDH levels were detected using a rabbit monoclonal GAPDH antibody (Cell Signaling 14C10 #2118) at 1:1000 and the same LICOR-compatible anti-rabbit IR secondary antibody at 1:5000 dilution.

EGLN1 and VHL inhibitors

EGLN1 inhibitors [IOX2 (Catalog No. S2919), Roxadustat FG-4592 (Catalog No. S1007), Molidustat Bay-85–3934 (Catalog No. S8138), FG-2216 (Catalog No. S7979), and Daprodustat GSK1278863 (Catalog No. S8171) were obtained from Selleck Chemicals (www.selleckchem.com). The VHL inhibitor VH298 was obtained from Tocris Bioscience (Catalog No. 6156). Compounds were dissolved in DMSO per manufacturer's instructions

to an initial stock concentration of 10 mM or formulated in 50% PEG for microdevice experiments.

Luciferase Competition Assay

Infections to make cell lines expressing ORFs for Firefly Luciferase 2P (gateway cloned into pLX_313 from Promega pGL4.11[FLuc2P]) and Renilla Luciferase (pLX_313) were performed by centrifuging freshly seeded plates containing cells with lentiviral particles and 4ug/mL polybrene for two hours at 2000 rpm. Cell lines expressing pLX_311-cas9 were infected with pLX_313-FireflyLuc2P and parental cell lines were infected with pLX_313-RenillaLuc. Firefly and Renilla expressing cells were mixed 1:1 in wells of a 96 well plate containing 4ug/mL polybrene. After mixing the cell population we added sgRNA lentivirus. Both firefly and Renilla expressing cells are infected with the sgRNA but only the firefly expressing cells have Cas9. Freshly seeded plates were spun at 2000 rpm for 30 min and incubated overnight at standard cell culture conditions. The following day, infected cells were selected using 4 ug/mL puromycin for 48 h. Every 3–4 days following the selection period, the plate is split into two new plates. One plate is read 24 h later using reagents from a Dual-Glo Luciferase Assay Kit (Promega). The other plate continues until the next time point. Luciferase signal was quantified using an Envision Plate Reader. Data was expressed as the fold change of the ratio of Firefly Luciferase signal to Renilla Luciferase signal normalized to the signal ratio post-selection from an infection with the empty sgRNA delivery vector (xPR_003) and averaged across 6 biological replicates. Results are representative of two independent experiments.

CellTiter-Glo Viability Assays

We performed CellTiter-Glo (CTG) viability assays per the manufacturer's instructions. Briefly, we seeded 5,000–10,000 cells per well in a 96 well plate then treated with either DMSO or EGLN1 inhibitor in doses indicated. Following 3–6 days treatment (retreated at day 4) we added CTG compound and measured viability. Data presented is the average of three technical replicates. Data is representative of three independent experiments.

Proliferation Assays

Non-Cas9 expressing cells were plated on a 12 well or 6 well plate in triplicate with varying concentrations of FG-4592. Every 3 – 4 days cells were trypsinized, counted using Nexcelom Cellometer, and reseeded at equal densities with the same concentrations of FG-4592, IOX2, BAY85–3934 or VH298. Data presented is the average of three technical replicate wells when available, excluding wells where there are no live cells to passage. Data is representative of two independent experiments.

Flow cytometry analysis

Flow cytometry was performed at the Broad Institute Flow Cytometry core using CFSE (5(6)-Carboxyfluorescein N-hydroxysuccinimidyl ester)– Cell Labeling Kit (Abcam ab113853) to label dividing cells with CFSE and analyzed on FL-1 Excitation(max) 492nm, Emission(max) 517nm. Apoptosis was detected using PE Annexin V Apoptosis Detection Kit 1 (BD Biosciences 559763). Dual labeling Annexin V with 7-Amino-Actinomycin(7-

AAD) allowed quantification of apoptosis. Data is presented as the average of two technical replicates and is representative of three independent experiments. Data was analyzed using FlowJo data analysis.

Hypoxia Response Element

The Hypoxia Response Element (HRE) was designed based on previous publications (18, 19) and was cloned with a luciferase reporter. The construct was then stably transfected to EGLN1 dependent and independent cell lines. Following transfection, cells were treated with EGLN1 inhibitor for up to 6 days and luciferase activity was measured as a readout of HIF1A activity.

Colony Formation Assay Dose Response Curves

Cells were plated at a low density (250 – 1000 cells/well) with varying concentrations of FG-4592 (Selleck) on 24 well plates. Media and drug were refreshed every 3–4 days for 10 days. Cells were fixed on the plate with 10% neutral buffered formalin (Thermo Fisher Scientific) and stained with 0.1% crystal violet in 10% ethanol. After plates were washed and dried, dye was extracted using 10% acetic acid. Absorbance of extracted dye samples at 595nm was quantified using a Molecular Devices SpectraMax M5 Plate Reader. Data presented is normalized to the DMSO treated sample. Data is representative of three independent experiments.

Animal Models

Female Athymic$^{Nu/Nu}$ mice (8–10 weeks old) were used and obtained from Jackson Laboratories and had access to food and water in appropriate housing conditions. All animal procedures performed at the Broad Institute were approved by the Institutional Animal Care and Use Committee (IACUC) and according to institutional regulations.

In vivo transplantation

Cells were infected with lentivirus expression control sgChr2–1 or sgEGLN1–9. Following 24 h of selection cells were subcutaneously implanted into recipient mice (athymic$^{Nu/Nu}$, Jackson Laboratories) in 50% matrigel at a concentration of 250,000 cells (ES2) or 400,000 cells (OVISE). Mice were implanted with sgChr2–1 and sgEGLN1–9 at opposite side flanks to control for any variability between mice. Following the detection of tumors, tumor size was quantified at least once per week using a caliper measuring tumor dimensions. Mice were euthanized at the end of the experiment. Tumors were harvested from the euthanized mice and dissociated in cell culture and further saved for RNA, protein or frozen cell storage.

RT-PCR

ES2-formed tumors harvested from implanted cells were isolated from total tumor. Total RNA was isolated using QIAGEN miRNeasy Mini Kits. Reverse transcription for RNA samples was performed using Thermo Fisher Superscript III First-Strand Synthesis System (Thermo Fisher #18080–051). RT-PCR was performed on the QuantStudio 6 Flex (Applied Biosystems) using SYBR Green Master Mix available from Thermo Fisher (Thermo Fisher

#4367659) with probes against EGLN1 deletion site in triplicate. Comparative CT was chosen for analysis and was normalized against RPS17 as an internal control.

RNA Sequencing

RNA sequencing was performing following 5-day treatment of EGLN1-dependent and independent cell lines in triplicate with either EGLN1 inhibitor or DMSO (control). Cell lines also had EGLN1 KO or Chr2–1 KO (control) and were allowed to grow for 7 days before cell pellets were collected and RNA was isolated using Qiagen Trizol (Qiazol) RNA extraction kit. Purified RNA was provided to RNA sequencing core at the Broad Institute and sequencing was performed on the Illumina HiSeq 2000 or HiSeq 25000 instruments with coverage of 100 million paired 101 nucleotides-long reads per sample. RNA reads were aligned using TopHat version 1.4 and Gene RPKM values were calculated using GTEx project pipeline.

Microdevice manufacturing and implantation

Devices were manufactured as previously described (23). Briefly, microscale devices at diameter 820uM and length 3mm were manufactured and pure powder compounds were formulated in 50% PEG. Mice were subcutaneously delivered ovarian cancer cells and tumors were allowed to grow to 1cm^2. Mice were anesthetized during implantation using 1% isoflurane. A 19-guage spinal biopsy needle (Angiotech) was inserted into the tumor and served as the location for the device to be implanted.

Immunohistochemistry

Immunohistochemistry was done on 4um serial sections from formalin-fixed, paraffin-embedded (FFPE) tumor tissues. The samples were deparaffinized, rehydrated, and pretreated for antigen retrieval by microwave treatment. Immunostaining was done using cell proliferation marker Ki67 and cleaved caspase 3 (CCE) at the Koch Institute Microscopy Core Facility.

Statistical Analysis

All experiments presented here are shown either as the average of at least 3 samples repeated twice and analyzed either with standard student's t-test or ANOVA as appropriate. Computational tests such as Gene Set Enrichment Analysis and TCGA statistical analysis were performed using computational software tools developed at the Broad Institute and Dana Farber Cancer Institute.

Results

Identification of EGLN1 as a druggable preferential dependency

Genes that are essential for cell viability in a context-specific manner, in contrast to pan-essential genes, represent potential cancer dependencies. To identify such genes, we have performed genome-scale loss-of-function screens using RNAi and CRISPR-Cas9 technologies in hundreds of human cancer cell lines (2, 3, 5). Our earlier analysis of the data derived from screening 501 human cancer cell lines with RNAi had identified 762 genes that

were essential for the proliferation/survival of a subset of cell lines at a level of 6 standard deviations from the mean dependency score (2, 3, 5); a stringent metric to find such differential dependencies. Of these 762 genes, we found that 153 were classified as druggable based on previous annotations [Figure 1A, Supplementary Table 2, (2)]. Among the druggable genes, 15 were targets of molecules that are either approved or in clinical trials. As expected, most of these compounds have been developed for oncology indications, providing proof of concept of using this approach in identifying cancer targets. In addition, we found one gene, *EGLN1* for which small molecule inhibitors are in phase II and III clinical trials to treat anemia in patients with chronic kidney disease (NCT03263091, NCT03303066, clinicaltrials.gov). We selected this target for further investigation as a candidate novel oncology therapeutic target.

To validate *EGLN1* dependency with an orthogonal technology to RNAi, we analyzed data derived from screening 436 cell lines using a genome-scale CRISPR-Cas9 library (7, 18). We found that *EGLN1* scored as a preferential dependency both in CRISPR and in RNAi datasets (Figure 1B, Supplementary Figure 1A–1C) (18–22). Indeed, the concordance between EGLN1 dependency in cell lines screened by CRISPR and RNAi was highly significant (Figure 1C, Pearson correlation 0.512, $p<10^{-17}$).

Since *EGLN1* is one of three family members, we queried whether the other family members, *EGLN2* and *EGLN3*, were also dependencies in any of the cell lines. We found that among the EGLN family members, *EGLN1* was the strongest preferential dependency in both CRISPR and RNAi datasets (Supplementary Figure 1A–1C). Furthermore, we found that there were few cell lines dependent on *EGLN1* that were also dependent on *EGLN2* or *EGLN3*.

We and others have previously shown that we could use co-dependencies derived from the Achilles datasets to identify genes that have similar function (2, 11–13, 24, 25). Here, we applied this method to gain insight into the molecular basis of *EGLN1* dependency. Specifically, we built linear models to identify co-dependency relationships between *EGLN1* and every other gene. We found that *VHL* was the strongest and most significantly associated dependency in the CRISPR-Cas9 screens, while *HIF1AN* were among the top hits in both CRISPR-Cas9 and RNAi and *HIF1A* was one of the strongest negatively associated hits (Figure 1D, Supplementary Figure 1D). These observations suggest that *EGLN1* dependency is related to its canonical function in the HIF pathway. To further investigate this association with members of the HIF pathway, we calculated the correlations between dependency profiles of every pair of genes in the pathway (*VHL, HIF1AN, HIF1A, HIF2A, EGLN1, EGLN2* and *EGLN3*). We found the strongest correlation within the pathway existed between EGLN1 dependency and VHL dependency followed by *EGLN1* dependency and *HIF1AN* (Hypoxia Inducible Factor 1 Alpha Subunit Inhibitor) dependency in CRISPR datasets (Figure 1E).

To understand why some cell lines are more dependent on EGLN1 than others, we next searched for genomic features, including gene expression, copy number alterations and mutations that related to EGLN1 dependency estimated from CRISPR and RNAi data (Supplementary Figure 1E–L, Supplementary Table 3, Supplementary Table 4). We found

that higher levels of *HIF1A* expression were among the most significantly associated gene expression features. In addition, in the reverse analysis, EGLN1 dependency was the top correlated dependency with *HIF1A* expression (Supplementary Figure 1M). In particular, we found that cell lines that express lower levels of *HIF1A* were not dependent on *EGLN1*, suggesting that high levels of expression might be required for a dependency (Figure 1F). Finally, when we interrogated which gene sets correlated with *EGLN1* dependency, we identified hypoxia-related gene sets among the top correlated gene sets (Supplementary Figure 1N, 1O). Taken together, all these observations are consistent with the hypothesis that EGLN1 regulation of HIF1A is the downstream event responsible for the dependency.

EGLN1 dependency is enriched in ovarian clear cell carcinoma

To investigate whether *EGLN1* dependency was enriched in specific cancer types, we performed a lineage enrichment analysis using Fisher's exact test. We found that melanoma and ovarian cell lines were significantly enriched for *EGLN1* dependencies in the CRISPR-Cas9 dataset (Supplementary Figure 2A, FDR<0.1). Specifically, among the ovarian cancer cell lines, we found that 13 of 33 (39%) ovarian cancer cell lines were dependent on EGLN1 (Figure 2A, 2B). Similarly, we found these cell lines were also dependent on *EGLN1* in RNAi dataset and cell lines in both datasets show strongly correlated *EGLN1* dependencies (Supplementary Figure 2C). Ovarian cancer represents a heterogeneous disease comprised of 4 major different subtypes (26–36). To determine whether *EGLN1* dependency was enriched in a specific subtype we grouped the ovarian cancer cell lines by historical pathological, molecular and histological subtypes [Supplementary Table 5, adapted from (31, 34, 36)]. We found that *EGLN1* dependency was significantly enriched in ovarian clear cell carcinoma lines compared to every other ovarian subtype (Figure 2C, $p<0.05$; Supplementary Figure 2D, $p<0.05$).

We next evaluated if the association of *EGLN1* dependency with high expression levels of *HIF1A* remained significant in ovarian cell lines. We found that EGLN1-dependent ovarian cancer cells express *HIF1A* at significantly higher levels than non-EGLN1-dependent cells in the CRISPR dataset (Figure 2D, $p < 0.005$). We found a similar relationship between *EGLN1* dependency scores and *HIF1A* expression in RNAi dataset (Supplementary Figure 2E). In particular, when subdivided by histological subtypes, we found that ovarian clear cell lines showed the highest group expression of *HIF1A* in CRISPR (Figure 2E, $p<0.05$) and RNAi datasets (Supplementary Figure 2E). These results are consistent with previous observations that *HIF1A* is overexpressed/activated in clear cell compared to other ovarian cancer subtypes (37, 38).

Higher levels of *HIF1A* and a hypoxia gene set were correlated with *EGLN1* dependency within the ovarian cell lines after performing single-sample Gene Set Enrichment Analysis (ssGSEA, Figure 2F, Supplementary Figure 2F), indicating that in ovarian cell lines *EGLN1* dependency is also related to its known function in the HIF1A pathway.

Validation of EGLN1 dependency

To validate and characterize the observed *EGLN1* dependency, we designed a series of sgRNAs to identify sgRNAs that effectively delete *EGLN1*. We selected an EGLN1-

dependent cancer cell line, ES2 (Figure 3A), and an EGLN1-independent cell line, TOV112D (Supplementary Figure 3A), from the panel of cell lines screened in Project Achilles. We chose three sgRNAs (EGLN1–1, EGLN1–8, and EGLN1–9) for subsequent *EGLN1* knockout experiments. We found that deleting *EGLN1* led to an increase in HIF1A and subsequently phosphorylated HIF1A (39, 40). We concluded that these selected *EGLN1* sgRNAs effectively targeted EGLN1.

To assess the consequences of EGLN1 inhibition, we measured cell proliferation. We found that expression of the negative control sgChr2–1 (sgRNA designed to target an intergenic region on Chromosome 2) did not affect cell proliferation. In contrast, depletion of EGLN1 using sgRNA EGLN1–9 led to a significant ($p<0.05$) decrease in cell proliferation in the EGLN1-dependent cell line ES2 (Figure 3B) but did not affect proliferation of the EGLN1-independent cell line, TOV112D (Figure 3C).

We hypothesized that EGLN1-dependent cells would also be dependent on *VHL*. To test this, we generated VHL-knockout cells using VHL-specific sgRNAs and confirmed loss of VHL by immunoblotting (Supplementary Figure 3B). We found that VHL-deficient cells showed a significant ($p<0.05$) decrease in population doublings (Figure 3D).

To assess the effects of depleting EGLN1 in a longer term assay, we performed a competition experiment in which we assessed whether cells with EGLN1 KO would be depleted over time when directly compared to cells expressing a control sgRNA (Figure 3E). Specifically, we introduced different sgRNAs in Renilla or Firefly+Cas9 expressing cells then determined the consequences of expressing each sgRNA by assessing Firefly/Renilla ratio over time. We performed the competition assay in three EGLN1-dependent cell lines (ES2, OVTOKO and OVISE) and two cell lines not dependent on EGLN1 (TOV112D and HEYA8). As a positive control for depletion of the cell population, we used sgRNAs targeting the RNA Polymerase II Subunit D (sgPOLR2D) and RNA Polymerase I Subunit C (sgPOLR1C). As negative controls, we used sgChr2–1 and sgLacZ. We found in ES2, OVTOKO and OVISE (EGLN1-dependent) that cells expressing an EGLN1-targeting sgRNA were depleted over time at a rate similar to cells expressing sgRNA targeting POlR2D or POLR1C (Figure 3E, top). Furthermore, when we performed this same experiment in EGLN1-independent cell lines, we found no difference between cells expressing the negative control sgRNA or sgRNA targeting *EGLN1* (Figure 3E, bottom). These observations confirm that depletion of EGLN1 leads to decreased cell proliferation in a subset of ovarian cancer cell lines.

Pharmacological inhibition of EGLN1 or VHL inhibits proliferation in a subset of cell lines

EGLN1 is a prolyl hydroxylase, and several PHD inhibitors have been described (41, 42), which prevent the degradation of HIF1A. Specifically, compound FG-4592, also known as Roxadustat, is currently being evaluated for the treatment of anemia in dialysis-dependent chronic kidney disease (CKD) and non-dialysis dependent CKD (42–45). We found that exposure of both ES2 and TOV112D to FG-4592 and the Bayer compound Molidustat (Bay 85–3934) led to increased HIF1A levels and phosphorylated HIF1A in a concentration-dependent manner (Figure 4A, Supplementary Figure 4A–4C). This accumulation was observed at 5–10 uM and peaked at 20–40 uM, consistent with the reported effective

concentrations of both compounds (43–47). These concentrations (5 uM-40 uM) were used for all subsequent experiments to test the effect of pharmacological inhibition of EGLN1 in EGLN1-dependent cells. In addition, we also tested HIF1A activity using a hypoxia-response element (HRE) fused to a luciferase reporter (Figure 4B) (48). Following treatment with FG-4592, we found that HIF1A activity was increased in both EGLN1-dependent cell lines and cell lines that are not EGLN1-dependent. However, when we compared HIF1A activity between both cell lines we found that the EGLN1-dependent cell line exhibited higher HIF1A activity (Figure 4B). This finding suggests that pharmacological inhibition of EGLN1 in EGLN1-dependent cell line induces higher activity of HIF1A than the cell line not dependent on EGLN1. We also found that FG-4592 reduced viability in ES2 over 48 hours while had no effect on TOV112D via Cell Titer Glo (CTG) assay in a dose-dependent manner (Figure 4C). To confirm these observations, we tested several other EGLN1 inhibitors FG-2216 (Fibrogen) and Daprodustat (GSK1278863 GlaxoSmithKline). We found that the EGLN1-dependent cell line ES2 showed sensitivity to all of these EGLN1 inhibitors (Supplementary Figure 4D). These observations confirm that inhibition of EGLN1 activity recapitulates the effects observed by deleting *EGLN1*.

To investigate if the observed decrease in cell number was due to apoptosis or cell cycle arrest, we treated cells for 3 days with FG-4592 and then labeled them with proliferation agent CFSE (Invitrogen) and analyzed proliferation by flow cytometry. We found that higher doses of FG-4592 reduced proliferation of ES2 but did not have a similar effect on TOV112D (Supplementary Figure 4E). Furthermore, we found a slight increase in apoptosis following three days of EGLN1 inhibition suggesting an initial cytotoxic effect (Supplementary Figure 4F). Thus, we found that short-term pharmacological inhibition of EGLN1 results in decreased proliferation. To evaluate the effect of FG-4592 on long-term proliferation, we carried out treatment of sensitive and resistant cells for up to 30 days. We found treatment with FG-4592 significantly reduced long term proliferation in sensitive cell lines (Figure 4D, Supplementary Figure 4G, 4H, $p<0.01$) but not insensitive cell lines (Figure 4E). Together, these observations show that EGLN1 inhibition reduces cell proliferation.

To further understand EGLN1 dependency, we tested the effect of EGLN1 inhibition in a low cell density colony formation assay. We found that EGLN1-dependent cell lines were sensitive to EGLN1 inhibition (Figure 4F, Supplementary Figure 4I) in a dose-dependent measurement. When we focused on cell lines that do not exhibit dependence on EGLN1, we found that increasing concentrations of FG-4592 did not have the same effect (Figure 4G, Supplementary Figure 4I). Together, these observations suggest that these cell lines are dependent on EGLN1 for colony-formation cell viability assays.

We hypothesized that EGLN1-sensitivity to small molecule inhibition would persist in the context of hypoxia. To test this hypothesis, we performed colony-forming formation assays in the context of normal culture conditions (normoxia) or in a hypoxic incubator at 5% oxygen (hypoxia). We found that EGLN1-dependent cells were sensitive to EGLN1 small molecule inhibitor FG-4592 in a dose-dependent manner in hypoxia and normoxia (Supplementary Fig. 4J). We did not observe an increased sensitivity to EGLN1 inhibition in

5% oxygen with the EGLN1-insensitive cell line TOV112D, suggesting that EGLN1 dependency persists under reduced oxygen concentrations *in vitro*.

Several inhibitors developed for clinical trials have the ability to target EGLN2 and EGLN3. To confirm that the effect that we observed was related to EGLN1 inhibition, we used the more selective EGLN1 inhibitor IOX2. We found in a short-term viability assay that IOX2-mediated inhibition of EGLN1 resembled FG-4592 inhibition of EGLN1 (Supplementary Figure 5A, 5B). Furthermore, when we looked at colony growth, we found EGLN1-dependent cell lines exhibited reduced dose-dependent colony growth compared to cell lines that were not dependent on EGLN1 (Supplementary Figure 5C). When we assessed the effect of IOX2 on long-term proliferation, we found that EGLN1-dependent cell lines showed decreased proliferation over time (Supplementary Figure 5D–5F). These findings suggest that the effects observed with FG-4592 and other EGLN clinical inhibitors is predominantly through inhibition of EGLN1, not EGLN2 or EGLN3.

We also hypothesized that pharmacological inhibition of VHL should mimic pharmacological inhibition of EGLN1. We used VH298 (Tocris), a novel chemical probe that is reported to block the interaction of VHL and HIF1A downstream of hydroxylation of HIF1A by EGLN1 (42), leading to HIF1A stabilization (Supplementary Figure 5G) and activation of HIF target genes. We found that treatment with VH298 substantially decreased cell proliferation in ES2 (Figure 4H) and slightly decreased proliferation in TOV112D (Figure 4I). We observed this effect in several other EGLN1-dependent cell lines (Supplementary Figure 5H, 5I). These findings suggested that EGLN1-dependent cells were more sensitive to VHL inhibition than EGLN1-independent cells.

Deletion of HIF1A rescues EGLN1 and VHL dependency

Based on our observation that *EGLN1* dependency was associated with higher expression of *HIF1A*, we hypothesized that depleting EGLN1 would affect HIF1A targets and pathways. We therefore performed RNA-sequencing in the EGLN1-dependent cell lines ES2 and OVISE with and without *EGLN1*. We found that among the genes that were differentially expressed (Supplementary Table 6, Supplementary Figure 6A), several genes act downstream of the EGLN1-HIF1A pathway. We next performed Gene Set Enrichment Analysis (GSEA) to identify significant changes in the EGLN1 knockout population. Within the top scoring pathways, we found enrichment in hypoxia and HIF1A-related pathways (Figure 5A, Supplementary Figure 6B). Together, these observations suggest that loss of EGLN1 strongly affects HIF1A-related pathways.

As HIF1A pathways were significantly affected by EGLN1 inhibition, we hypothesized that knockout of *HIF1A* would rescue EGLN1 dependency. We designed several sgRNAs targeting *HIF1A* and selected three that efficiently depleted HIF1A in EGLN1-sensitive cell line ES2 (Figure 5B). We found that deletion of *HIF1A* failed to affect the proliferation of EGLN1-insensitive cell lines. However, we found that depletion of HIF1A rescued EGLN1-sensitivity in ES2 (Figure 5C) and OVISE (Figure 5D) to FG-4592 ($p<0.05$). These observations suggest that the observed dependence of EGLN1 requires HIF1A.

Since *HIF1A* knockout rescued EGLN1 dependency, we hypothesized that HIF1A knockout may rescue VHL dependency. When compared to DMSO-treated control,) we found that knockout of HIF1A rescued cell proliferation blocked by VHL inhibitor VH298 (Figure 5E, $p<0.05$), suggesting that VHL-dependency functioned through the regulation of HIF1A.

Genetic and pharmacological inhibition of EGLN1 reduces tumor growth

We then tested whether depletion of EGLN1 affected tumor growth in vivo. Specifically, we used cells expressing sgRNAs against *EGLN1* or Chr2–1 (negative control) and subcutaneously implanted these into recipient mice (Figure 6A). We implanted control and knockout cells into opposite flanks of the same mouse to control for any tumor variation between mice. We found that *EGLN1* knockout significantly reduced tumor size over time in ES2 (Figure 6B). Furthermore, we found that OVISE tumor cells with deleted EGLN1 grew slower than OVISE tumors in which *EGLN1* was expressed (Figure 6C). When we looked at the RNA expression of a subset of the tumors that had grown in ES2 cells with inhibited EGLN1, we found a correlation with *EGLN1* expression and tumor size (Figure 6D), suggesting that inactivation of the EGLN1 gene significantly inhibits tumor growth.

To determine if pharmacological inhibition of EGLN1 also inhibited tumor growth, we used an implantable microdevice to directly deliver multiple compounds to different parts of the tumor (23). By inserting this microdevice directly into the tumor, we assessed the effect of FG-4592, and VH298 in tumors *in vivo*. Specifically, we implanted ES2 cells with intact HIF1A (ES2) or HIF1A knockout (ES2 HIF1A KO) in immunodeficient mice and allowed the tumors to grow to 1 cm^2 before implanting a microdevice containing the EGLN1 inhibitor FG-4592 and VHL inhibitor VH298. Following implantation, we collected the tumors after 48 hours and sectioned and stained the tumors for proliferation with an antibody against Ki-67, a cellular marker for proliferating cells, or Cleaved Caspase-3, a cellular marker for apoptosis. As expected, local delivery of PEG (polyethylene glycol, the vehicle used for drug formulation) had no effect on cell proliferation or apoptosis, demonstrated by clear immunostaining of Ki-67 (Figure 6E, Supplementary Figure 7, top) in both HIF1A WT or HIF1A KO tumors. We found that addition of doxorubicin reduced proliferation and increases apoptosis in both HIF1A WT and HIF1A KO cells (Figure 6E, Supplementary Figure 7, top middle). Consistent with our previous *in vitro* data (Figure 4), we found that pharmacological inhibition of EGLN1 causes a dramatic reduction in proliferating cells and increased apoptosis in the region of tumor exposed to the local microdevice delivery of FG-4592 (Figure 6E, Supplementary Figure 7, bottom middle), while knockout of HIF1A exhibited no change in proliferation or apoptosis upon local delivery of FG-4592. Similarly, we found addition of VH298 resulted in the reduction of proliferating cells and increased apoptosis which was also dependent on intact HIF1A (Figure 6E, Supplementary Figure 7, bottom). These data collectively demonstrate that genetic and pharmacological perturbation of EGLN1 reduces tumor burden, cell proliferation and increase apoptosis *in vivo* and that this effect requires HIF1A.

Discussion

Under normal conditions, EGLN1 functions to hydroxylate HIF1A and target it for ubiquitination and subsequent degradation by VHL (Figure 7A). Here we show that in a subset of clear cell ovarian cancer and melanomas, genetic knockout or pharmacological inhibition of EGLN1 stabilizes HIF1A and inhibits proliferation (Figure 7B). Similarly, genetic knockout or pharmacological inhibition of VHL prevents HIF1A ubiquitination and degradation which results in HIF1A stabilization and, subsequently, a decrease in proliferation (Figure 7C). Deletion of *HIF1A* rescues both EGLN1 dependency and VHL dependency (Figure 7D). Pharmacological inhibition of EGLN1 recapitulated the effects of genetic suppression of EGLN1, both in vitro and in vivo, suggesting that EGLN1 inhibition is a potential therapeutic strategy in these tumors.

As expected, genetic deletion of *EGLN1* led to HIF1A accumulation (Figure 3A), which in turn led to a decrease in proliferation (Figure 3B) and reduced fitness in our competition assay compared to EGLN1-functional cells (Figure 3E). After pharmaceutical inhibition of EGLN1 we observed similar accumulation of HIF1A and increased HIF1A activity (Figure 4A, Figure 4B). While EGLN1 has been described both as an oncogene and a tumor suppressor (39, 45, 49–53), a specific dependency of a subset of cancers on *EGLN1* has not been reported. Jokilehto et al. (39) found that *EGLN1* expression was strongly associated with highly proliferative head and neck squamous cell carcinomas (HNSCC). Furthermore, Klotzsche-von Ameln et al. found EGLN1 inhibition led to a decrease in tumor growth using mouse lung cancer cell line LLC and osterocarcoma line LM8 (51). Conversely, Chan et al. found that low PHD2 expression in colorectal cancers correlated with poorer survival, and experiments in cell line models showed that low PHD2 expression correlated with increased tumor vasculature (52). Bordoli et al. observed decreased EGLN1 was associated with increased tumor growth through increased VEGF, Amphiregulin and IL-8 (53). Thus, EGLN1 is another of a growing number of genes that can act both as an oncogene and tumor suppressor gene depending on the context (54).

Our findings suggest that increased HIF1A decreases the fitness of EGLN1-dependent cells. Specifically, we found that inactivation of EGLN1, using either genetic or pharmacologic means, resulted in a pronounced decrease in proliferation. We observed that this decrease in proliferation coincided with stabilization of HIF1A. Thus, we hypothesized that HIF1A loss could rescue EGLN1-mediated death. Indeed, we found that EGLN1-dependent cell lines were rendered insensitive to EGLN1 inhibition by loss of HIF1A (Figure 5C, Figure 5D). Together, these observations demonstrate that EGLN1 dependency requires HIF1A expression.

We found that a large number of cell lines dependent on *VHL* (Supplementary Figure 1A). We also found that cell lines dependent on *EGLN1* were also dependent on *VHL* (Figure 3D, Figure 4H, Supplementary Figure 5H, 5I). While all the EGLN1-dependent cell lines were also dependent on VHL in the CRISPR dataset (Figure 1D, Figure 1E), we were surprised to observe VHL scored as an essential gene (Supplementary Figure 1A). As VHL is downstream of EGLN1 and directly responsible for the ubiquitination and degradation of HIF1A (16, 17, 40–42) one possible hypothesis for this observation is that loss of VHL can

drive stabilization and accumulation of HIF1A in cell lines. We found that dependency on VHL in EGLN1-dependent cell lines was dependent on functional HIF1A. Similar to our previous observations with EGLN1 dependency, knockout of *HIF1A* rescues VHL dependency (Figure 5E). This finding suggests VHL also functions as a cancer dependency in EGLN1-dependent cells through negative regulation of HIF1A.

Previous reports found that overexpression of *HIF1A* has been associated with multiple tumor types, and tumors in hypoxia are known to require HIF1A to survive (14–17). However, other reports have also implicated HIF1A as a negative regulator of proliferation (49–51). There are a several hypotheses that could explain these observations. First, the observed effects of activating HIF1A may be tumor-type specific. In our initial analysis, we found significant enrichment in of EGLN1 dependency in melanoma and clear cell ovarian cancer. Indeed, these clear cell ovarian cancer cell lines died when HIF1A expression was stabilized.

Alternatively, it was possible that the observed difference in sensitivity involved whether the cells experienced hypoxia. However, we found under conditions of 5% oxygen that EGLN1 dependent cells were still susceptible to EGLN1 inhibition. Furthermore, when we examined *in vivo* growth of tumors under presumably hypoxic conditions, we found that genetic knockout and small molecule inhibition of EGLN1 reduced tumor growth and suppressed proliferation. These findings suggest that cell line dependence on EGLN1 is independent of hypoxia.

The standard therapeutic procedure to clear cell ovarian cancer remains surgical cytoreduction and subsequent chemotherapy using platinum agents and taxane (55). Clear cell ovarian cancers, compared to other histological ovarian subtypes, are resistant to chemotherapy (55). Thus, targeted therapy has been proposed, and the need for potential targets and therapy is pressing. EGLN1 inhibitors are in clinical trials for anemia in patients with chronic kidney disease (CKD) (43–45). Our observations suggest that these inhibitors may also be useful in EGLN1-dependent cancers. Our data suggest that cancers with low *HIF1A* expression would not respond to EGLN1 therapy, while a subset of patients with high *HIF1A* expression would respond. This association was stronger in melanoma and extremely strong in clear cell ovarian cancer cells. Previous work has shown that clear cell ovarian cancer patients have higher expression of HIF1A (37, 38). Thus, these patients would be the ideal patient population to assess the efficacy of EGLN1-targeted therapy in cancers.

Supplementary Material

Refer to Web version on PubMed Central for supplementary material.

Acknowledgements

We would like to thank Nancy Dumont (Broad Institute) for her suggestions and feedback on all *in vivo* experiments and William G. Kaelin Jr and his lab for materials provided and advice on experiments. This work was supported by the National Institute of Health/National Cancer Institute U01 CA176058 (W.C.H.), the H.L. Snyder Foundation (W.C.H.), National Cancer Institute Training Grant 5T32 CA009361–35 (C.P.) and the Carlos Slim Foundation in Mexico through the Slim Initiative for Genomic Medicine (F.V.).

Biography

W.C.H. is a consultant for Thermo Fisher, AjuIB, MPM Capital and Parexel and is a founder and serves on the scientific advisory board for KSQ Therapeutics.

References

1. Barrangou R et al., Advances in CRISPR-Cas9 genome engineering: lessons learned from RNA interference. Nucleic Acids Res. 43, 3407–19 (2015) [PubMed: 25800748]
2. Tsherniak A et al., Defining a Cancer Dependency Map. Cell 170, 564–576 (2017) [PubMed: 28753430]
3. Root DE, Hacohen WC Fau N et al., Genome-scale loss-of-function screening with a lentiviral RNAi library. Nat Methods 17, 715–9 (2006)
4. Shalem O, Sanjana NE, Zhang F, High-throughput functional genomics using CRISPR-Cas9. Nature reviews. Genetics 16, 299–311 (2015).
5. McDonald ER 3rd et al., Project DRIVE: A Compendium of Cancer Dependencies and Synthetic Lethal Relationships Uncovered by Large-Scale, Deep RNAi Screening. Cell 170, 577–592 (2017) [PubMed: 28753431]
6. Sanchez-Rivera FJ, Jacks T, Applications of the CRISPR-Cas9 system in cancer biology. Nat Rev Cancer. 15, 387–95 (2015) [PubMed: 26040603]
7. Meyers et al., Computational correction of copy number effect improves specificity of CRISPR-Cas9 essentiality screens in cancer cells. Nat Genet 49, 1779–1784 (2017) [PubMed: 29083409]
8. Peng J, Zhou Y, Zhu S, Wei W, High-throughput screens in mammalian cells using the CRISPR-Cas9 system. FEBS J. 282, 2089–96 (2015) [PubMed: 25731961]
9. Kim DU et al., Analysis of a genome-wide set of gene deletions in the fission yeast Schizosaccharomyces pombe. Nat Biotechnol 28, 617–623 (2010) [PubMed: 20473289]
10. Zhan T, Boutros M, Towards a compendium of essential genes – From model organisms to synthetic lethality in cancer cells. Critical Reviews in Biochemistry and Molecular Biology 51, 74–85 (2016). [PubMed: 26627871]
11. Luo B et al., Highly parallel identification of essential genes in cancer cells. Proc Natl Acad Sci U S A 105, 20380–5 (2008) [PubMed: 19091943]
12. Cheung HW et al., Systematic investigation of genetic vulnerabilities across cancer cell lines reveals lineage-specific dependencies in ovarian cancer. Proc Natl Acad Sci U S A 108, 12372–7 (2011) [PubMed: 21746896]
13. Paolella B et al., Copy-number and gene dependency analysis reveals partial copy loss of wild-type SF3B1 as a novel cancer vulnerability. LID - 10.7554/eLife.23268 [doi] LID - e23268 [pii].
14. Berra E et al., HIF prolyl-hydroxylase 2 is the key oxygen sensor setting low steady-state levels of HIF-1α in normoxia. The EMBO Journal 22, 4082–4090 (2003). [PubMed: 12912907]
15. Tennant DA et al., Reactivating HIF prolyl hydroxylases under hypoxia results in metabolic catastrophe and cell death. Oncogene 28, 4009–21 (2009) [PubMed: 19718054]
16. Kaelin WG, The VHL Tumor Suppressor Gene: Insights into Oxygen Sensing and Cancer. Transactions of the American Clinical and Climatological Association 128, 298–307 (2017). [PubMed: 28790514]
17. To KK, Huang LE, Suppression of hypoxia-inducible factor 1alpha (HIF-1alpha) transcriptional activity by the HIF prolyl hydroxylase EGLN1. J Biol Chem 280, 38102–7 (2005) [PubMed: 16157596]
18. Cancer Data Science. Broad Institute Cancer Dependency Map, CRISPR Avana Dataset 18Q2 (Avana_public_18Q2). figshare. 10.6084/m9.figshare.6205118.v1 (2018).
19. Aguirre AJ et al., Genomic Copy Number Dictates a Gene-Independent Cell Response to CRISPR/Cas9 Targeting. Cancer Discov 6, 914–29 (2016) [PubMed: 27260156]
20. Cancer Data Science. DEMETER2 data. figshare 10.6084/m9.figshare.6025238.v4 (2018).

21. McFarland JM et al., Improved estimation of cancer dependencies from large-scale RNAi screens using model-based normalization and data integration. Nature Communications 9, 4610bioRxiv, (2018).
22. Cancer Cell Line Encyclopedia Consortium, and Genomics of Drug Sensitivity in Cancer Consortium. 2015 Pharmacogenomic Agreement between Two Cancer Cell Line Data Sets. Nature 528 (7580):84–87. 10.1038/nature15736. [PubMed: 26570998]
23. Jonas O et al., An implantable microdevice to perform high-throughput in vivo drug sensitivity testing in tumors. Science translational medicine 7, 284ra257–284ra257 (2015).
24. Kim JW et al., Characterizing genomic alterations in cancer by complementary functional associations. Nat Biotechnol 34, 539–46 (2016) [PubMed: 27088724]
25. Howard TP et al., Functional Genomic Characterization of Cancer Genomes. Cold Spring Harb Symp Quant Biol 81, 237–246 (2016) [PubMed: 27815544]
26. Kaur T, Slavcev SD Fau - Wettig Ra, Wettig SD, Addressing the challenge: current and future directions in ovarian cancer therapy. Curr Gene Ther 9, 434–58 (2009) [PubMed: 20021329]
27. Anglesio MS, Carey MS, Köbel M, MacKay H, Huntsman DG, Clear cell carcinoma of the ovary: A report from the first Ovarian Clear Cell Symposium, June 24th, 2010. Gynecologic Oncology 121, 407–415.
28. Chan JK et al., Do clear cell ovarian carcinomas have poorer prognosis compared to other epithelial cell types? A study of 1411 clear cell ovarian cancers. Gynecologic Oncology 109, 370–376.
29. Yamaguchi K et al., Epigenetic determinants of ovarian clear cell carcinoma biology. Int J Cancer 135, 585–97 (2014) [PubMed: 24382740]
30. Lengyel E et al., Epithelial ovarian cancer experimental models. Oncogene 33, 3619–33 (2014) [PubMed: 23934194]
31. Haley J et al., Functional characterization of a panel of high-grade serous ovarian cancer cell lines as representative experimental models of the disease. Oncotarget 7, 32810–20 (2016) [PubMed: 27147568]
32. Ahmed N, Stenvers KL, Getting to know ovarian cancer ascites: opportunities for targeted therapy-based translational research. Front Oncol 23, 256 (2013)
33. Jayson GC, Kohn EC, Kitchener HC, Ledermann JA, Ovarian cancer. Lancet 384, 1376–88 (2014) [PubMed: 24767708]
34. Beaufort CM et al., Ovarian Cancer Cell Line Panel (OCCP): Clinical Importance of In Vitro Morphological Subtypes. PLOS ONE 9, e103988 (2014). [PubMed: 25230021]
35. Lim D, Oliva E, Precursors and pathogenesis of ovarian carcinoma. Pathology 45, 229–242 (2013). [PubMed: 23478230]
36. Anglesio MS et al., Type-Specific Cell Line Models for Type-Specific Ovarian Cancer Research. PLOS ONE 8, e72162 (2013). [PubMed: 24023729]
37. Lee S, Garner WR Fau - Welch Ei, Welch RS Fau - Berkowitz Wr, Berkowitz SC Fau - Mok Rs, Mok SC, Over-expression of hypoxia-inducible factor 1 alpha in ovarian clear cell carcinoma. Gynecol Oncol 106, 311–7 (2007) [PubMed: 17532031]
38. Osada R et al., Expression of hypoxia-inducible factor 1alpha, hypoxia-inducible factor 2alpha, and von Hippel-Lindau protein in epithelial ovarian neoplasms and allelic loss of von Hippel-Lindau gene: nuclear expression of hypoxia-inducible factor 1alpha is an independent prognostic factor in ovarian carcinoma. Hum Pathol 38, 1310–20 (2007) [PubMed: 17555795]
39. Jokilehto T et al., Overexpression and nuclear translocation of hypoxia-inducible factor prolyl hydroxylase PHD2 in head and neck squamous cell carcinoma is associated with tumor aggressiveness. Clin Cancer Res 12, 1080–7 (2006) [PubMed: 16489060]
40. Aprelikova O et al., Regulation of HIF prolyl hydroxylases by hypoxia-inducible factors. J Cell Biochem 92, 491–501 (2004) [PubMed: 15156561]
41. Ivan M, Kaelin WG Jr., The EGLN-HIF O2-Sensing System: Multiple Inputs and Feedbacks. Mol Cell 66, 772–779 (2017) [PubMed: 28622522]
42. Frost J et al., Potent and selective chemical probe of hypoxic signaling downstream of HIF-alpha hydroxylation via VHL inhibition. Nature Communications 7, 13312 (2016).

43. Del Vecchio L, Locatelli F, Roxadustat in the treatment of anaemia in chronic kidney disease. Expert Opin Investig Drugs 27, 125–133 (2018)
44. Besarab A et al., Randomized placebo-controlled dose-ranging and pharmacodynamics study of roxadustat (FG-4592) to treat anemia in nondialysis-dependent chronic kidney disease (NDD-CKD) patients. Nephrol Dial Transplant 30, 1665–73 (2015) [PubMed: 26238121]
45. Provenzano R et al., Roxadustat (FG-4592) Versus Epoetin Alfa for Anemia in Patients Receiving Maintenance Hemodialysis: A Phase 2, Randomized, 6- to 19-Week, Open-Label, Active-Comparator, Dose-Ranging, Safety and Exploratory Efficacy Study. American Journal of Kidney Diseases 67, 912–924 (2016). [PubMed: 26846333]
46. Buisson C et al., Detection by LC–MS/MS of HIF stabilizer FG-4592 used as a new doping agent: Investigation on a positive case. Journal of Pharmaceutical and Biomedical Analysis 121, 181–187 (2016). [PubMed: 26808067]
47. Jain IH et al., Hypoxia as a therapy for mitochondrial disease. Science 352, 54–61 (2016) [PubMed: 26917594]
48. Gao S, Zhou J, Zhao Y, Toselli P, Li W, Hypoxia-response element (HRE)-directed transcriptional regulation of the rat lysyl oxidase gene in response to cobalt and cadmium. Toxicological sciences : an official journal of the Society of Toxicology 132, 379–389 (2013). [PubMed: 23161664]
49. Shen C et al., Genetic and functional studies implicate HIF1alpha as a 14q kidney cancer suppressor gene. Cancer Discov 1, 222–35 (2011) [PubMed: 22037472]
50. Chiavarina B et al., HIF1-alpha functions as a tumor promoter in cancer associated fibroblasts, and as a tumor suppressor in breast cancer cells: Autophagy drives compartment-specific oncogenesis. Cell Cycle 9, 3534–51 (2010) [PubMed: 20864819]
51. Klotzsche-von Ameln A, et al., Inhibition of HIF prolyl hydroxylase-2 blocks tumor growth in mice through the antiproliferative activity of TGFβ. Cancer Res 71(9), 3306–16 (2011) [PubMed: 21436457]
52. Chan DA et al., Tumor vasculature is regulated by PHD2-mediated angiogenesis and bone marrow-derived cell recruitment. Cancer Cell 15(6), 527–38 (2009) [PubMed: 19477431]
53. Bordoli MR et al., Prolyl-4-hydroxylase PHDS2- and hypoxia-inducible factor 2-dependent regulation of amphiregulin contributes to breast tumorigenesis. Onocogene 30(3) 548–60 (2011)
54. Winslow MM et al., Suppression of lung adenocarcinoma progression by Nkx2–1. Nature 473 101–4 (2011) [PubMed: 21471965]
55. Cobb LP and Gershenson DM Treatment of Rare Epithelial Ovarian Tumors Hematol Oncol Clin North Am 32 1011–1024 (2018) [PubMed: 30390757]

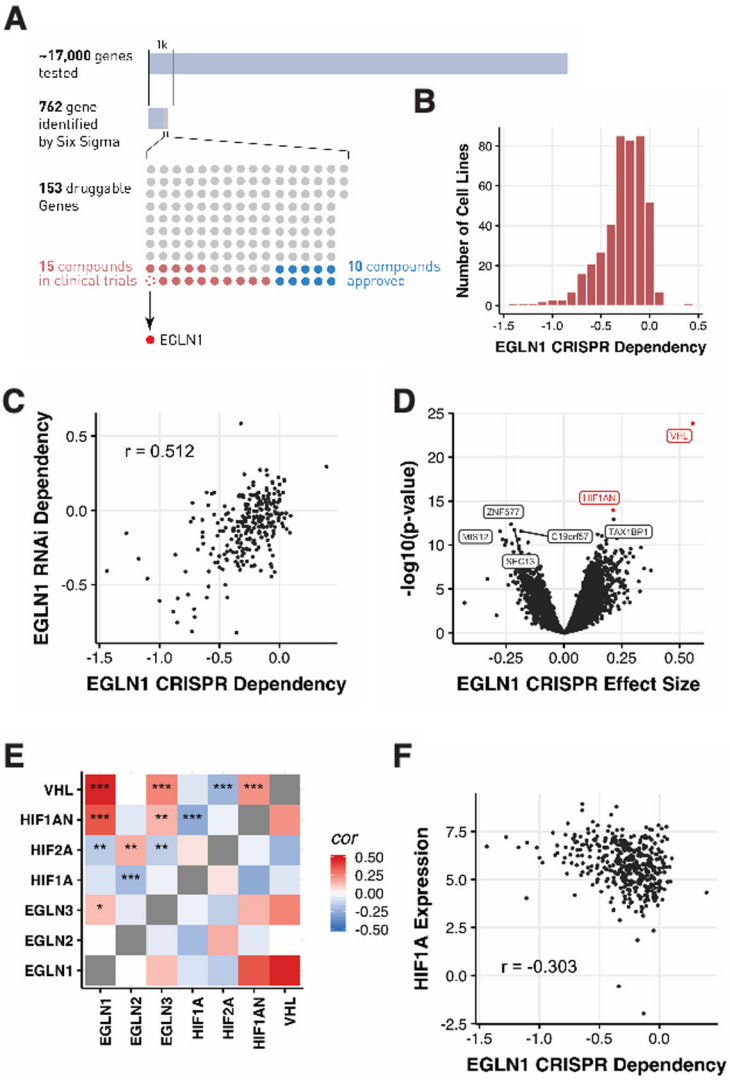

Figure 1. Identification of EGLN1 as a preferential cancer cell dependency.

A. Identification of EGLN1 dependency in RNAi data from Project Achilles. From the initial ~17k genes tested, we found 762 were strong (Six Sigma) dependencies using DEMETER scores. From these dependencies, we found 153 were currently druggable, while 15 of them had compounds in clinical trials. We identified EGLN1 as one of these 15 clinically druggable dependencies.

B. Identification of cancer cells dependent on EGLN1 using CRISPR-Cas9 data from Project Achilles. Histogram shows the distribution of EGLN1 CERES dependencies (X-axis) across 436 cancer cell lines screened with CRISPR. The left tail shows that a subset of lines are preferentially dependent on EGLN1.

C. Concordance between RNAi and CRISPR-Cas9 datasets. EGLN1 DEMETER2 scores are graphed against EGLN1 CERES scores (CRISPR, X-axis) for the 243 cell lines screened in both datasets. The correlation between the datasets was strong and highly significant. Pearson = 0.512. n=243, $p<10^{-21}$.

D. Volcano plot showing cancer dependencies associated with EGLN1 dependency graphed as p-value (-log10, Y-axis) against effect size (X-axis). Colored in red are other members of the EGLN1 pathway.

E. EGLN1 and VHL are the strongest correlated dependencies within the EGLN1 pathway while EGLN1 and HIF1AN are the second strongest correlated dependencies. P-values were adjusted using the Benjamini and Hochberg FDR method. FDR < 0.05 (*), 0.01 (**), 0.001 (***).

F. Cell lines that express low levels of HIF1A (Y-axis) are not dependent on EGLN1 (X-axis).

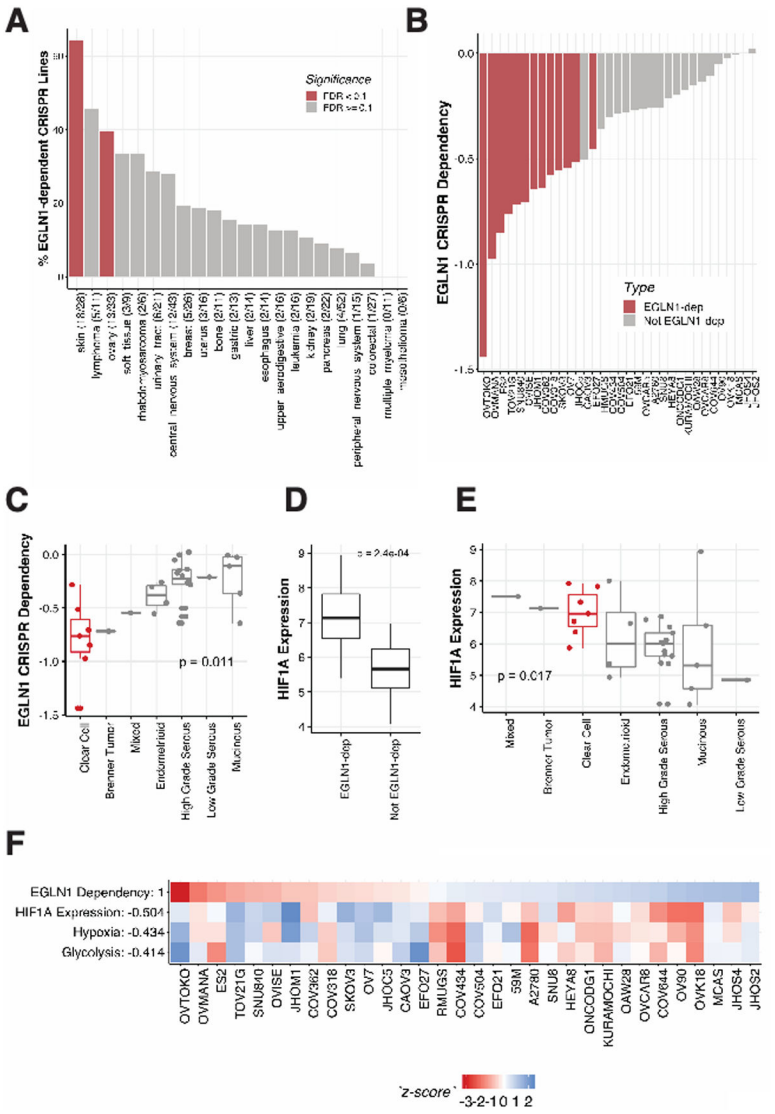

Figure 2. EGLN1 dependency is enriched in clear cell ovarian cancer and melanoma and associated with high HIF1A levels

A. Ovarian and melanoma cancer cell lines are enriched for EGLN1 dependencies in CRISPR screens. The percentage of EGLN1-dependent lines is graphed for each lineage. Significantly enriched lineages found by lineage enrichment analysis are colored in red. Note that lung lines are also significant, but are negatively enriched for EGLN1 dependencies.

B. Distribution of EGLN1 CERES scores (Y-axis) in ovarian cancer cell lines. 13 out of 33 cell lines screened in CRISPR Cell lines have a greater than 50% probability of being dependent on EGLN1. *CAOV3 is not identified as an EGLN1-dependency, despite having a lower CERES effect score than EGLN1-dependent line EFO27, because the screen quality and other cell-line-specific differences are reflected in the CERES probabilities of dependency.

C. CRISPR EGLN1 dependencies are enriched in clear cell ovarian cancer. A two-sample t-test of clear cells vs. all other ovarian subtypes reveals that clear cells are significantly enriched for EGLN1 dependencies ($p < 0.05$).

D. EGLN1-dependent cell lines (n = 13) express significantly more HIF1A (Y-axis) than non-EGLN1-dependent lines (n = 20) in CRISPR. Two-sample t-test p-value < 0.01.

E. Clear cell ovarian cancer cell lines have high HIF1A expression compared to all other ovarian lines. Two-sample t-test p-value $p<0.05$.

F. ssGSEA (single sample Gene Set Enrichment Analysis) reveals that EGLN1 dependency is associated with HIF1A-related pathways. Pearson correlations of EGLN1 dependency with each profile (Y-axis) were calculated, and z-score normalized profiles are shown.

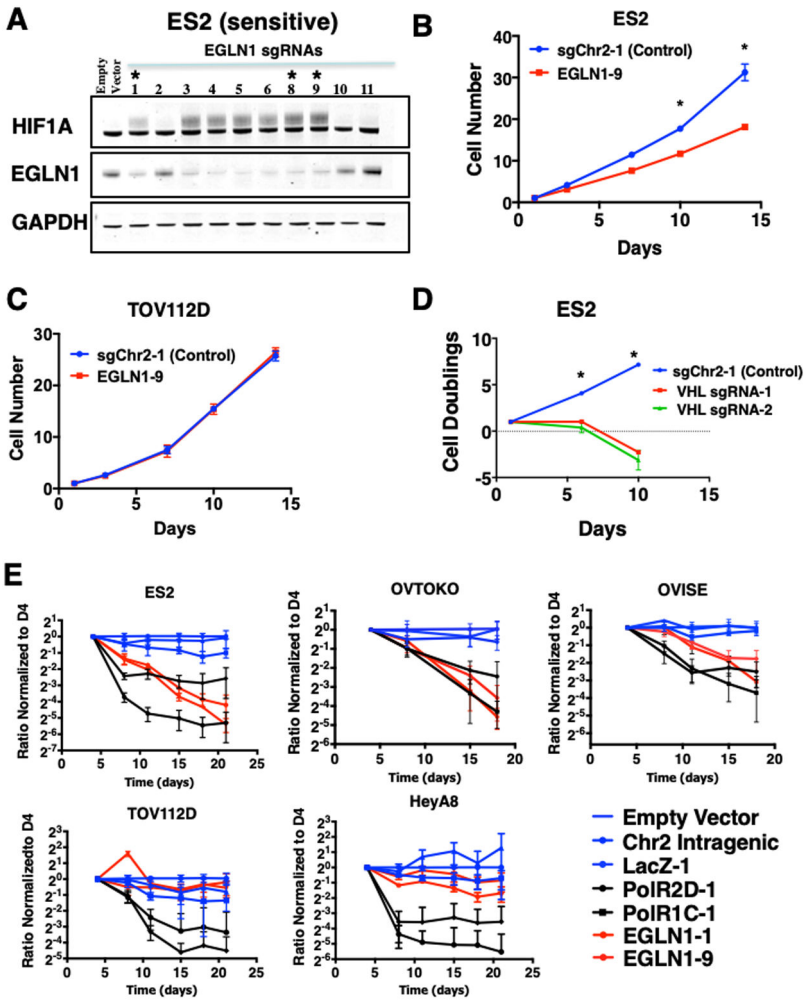

Figure 3. EGLN1 deletion inhibits proliferation in EGLN1-dependent cell lines.

A. Effects of EGLN1 deletion on HIF1A levels. Whole cell lysates of ES2-Cas9 with the indicated sgRNAs. Equal amounts of protein were analyzed by immunoblotting with GAPDH included as a marker of equal loading. Deletion of EGLN1 leads to increased HIF1A phosphorylation. *sgRNAs used for subsequent experiments.

B. EGLN1 deletion reduces proliferation in EGLN1-dependent cells. Cells were serially passaged every 3–4 days. Results are representative of 3 independent experiments and data is graphed as mean ± standard deviation of 3 replicates. *$p<0.05$

C. EGLN1 deletion does not affect proliferation in EGLN1 independent cells. Cells were serially passaged every 3–4 days. Results are representative of 3 independent experiments and data is graphed as mean ± standard deviation of 3 replicates.

D. VHL deletion reduces proliferation in EGLN1-dependent cells. Results are representative of 2 independent experiments and data is graphed as mean ± standard deviation of 3 replicates. *$p<0.05$

E. Luciferase competition assay. Renilla-expressing and Firefly+Cas9-expressing cells are mixed at 1:1 and then sgRNAs are expressed. Ratio of Renilla/Firefly luciferase was quantified, and cells were serially passaged every 3–4 days. EGLN1 KO cells (red) were compared to negative controls (blue) and positive controls (black). EGLN1 deleted cells

dependent on EGLN1 are outcompeted by EGLN1 WT cells over time in a proliferation assay, whereas EGLN1 deleted cells insensitive to EGLN1 are not. Results are representative of 2 independent experiments and data is graphed as mean ± standard deviation of 3 technical replicates. Empty Vector – Empty Vector with no sgRNA, Chr2 Intragenic – sgRNA targeting intergenic region of chromosome 2, LacZ-1 – sgRNA targeting LacZ gene, PolR2D-1 – sgRNA targeting RNA Polymerase 2 Subunit D, PolR1C-1 – sgRNA targeting RNA Polymerase 1 Subunit C.

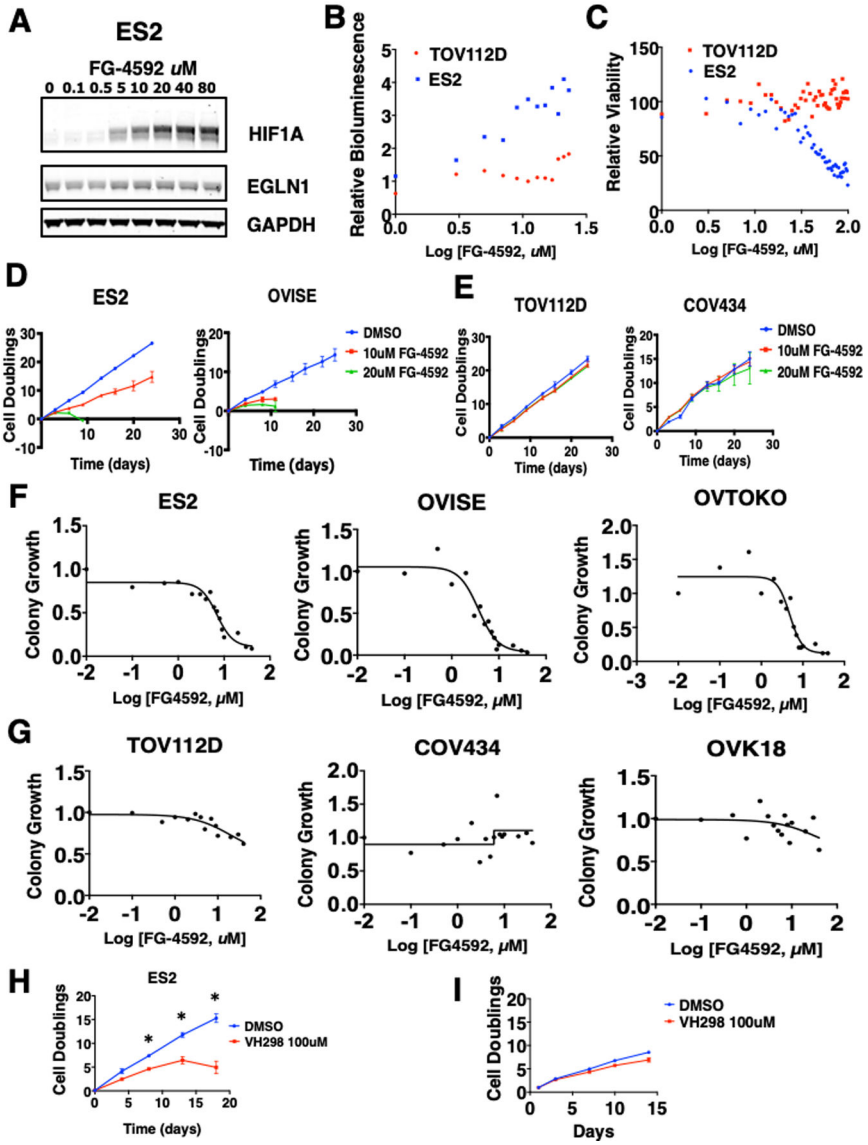

Figure 4. Inhibiting EGLN1 increases HIF1A expression and reduces proliferation in EGLN1-dependent cells.

A. Immunoblot showing that pharmaceutical inhibition(FG-4592) of EGLN1 increases HIF1A levels in a dose-dependent manner.

B. EGLN1 inhibitor increases HIF1A activity measured by using a Hypoxia Response Element (HRE) fused to a luciferase reporter. Luciferase activity was measured 48 hours post treatment with increasing dose of FG-4592. Data is representative of two independent experiments.

C. EGLN1 inhibitor reduces viability selectively in EGLN1-dependent cells. Cells were treated for 48 hours with increasing dose of FG-4592 (X-axis). Cell viability (Y-axis) was measured using CellTiter-Glo. The data shown is representative of three independent experiments.

D. EGLN1 inhibitor reduces long term proliferation in EGLN1-dependent cells. Results are representative of 3 independent experiments and data is graphed as mean ± standard deviation of 3 replicates.

E. EGLN1 inhibitor does not affect long term proliferation of EGLN1-insensitive cells. Results are representative of 3 independent experiments and data is graphed as mean ± standard deviation of 3 replicates.

F. EGLN1 inhibition reduces colony formation in a dose-dependent manner in EGLN1-dependent cells. Colonies were quantified as absorbance (Y-axis) over drug concentration (X-axis) over 10 days of treatment normalized to DMSO. Results are representative of 3 independent experiments.

G. EGLN1 inhibition has no significant effect on colony formation in EGLN1-insensitive cells. Colonies were quantified as absorbance (Y-axis) over drug concentration (X-axis) over 10 days of treatment normalized to DMSO. Results are representative of three independent experiments.

H. VHL inhibition reduces proliferation of EGLN1-dependent cells. Results are representative of 3 independent experiments, and data is graphed as mean ± standard deviation of 3 replicates. *$p<0.05$

I. VHL inhibition does not affect proliferation of EGLN1-insensitive cells. Results are representative of 2 independent experiments, and data is graphed as mean ± standard deviation of biological triplicates.

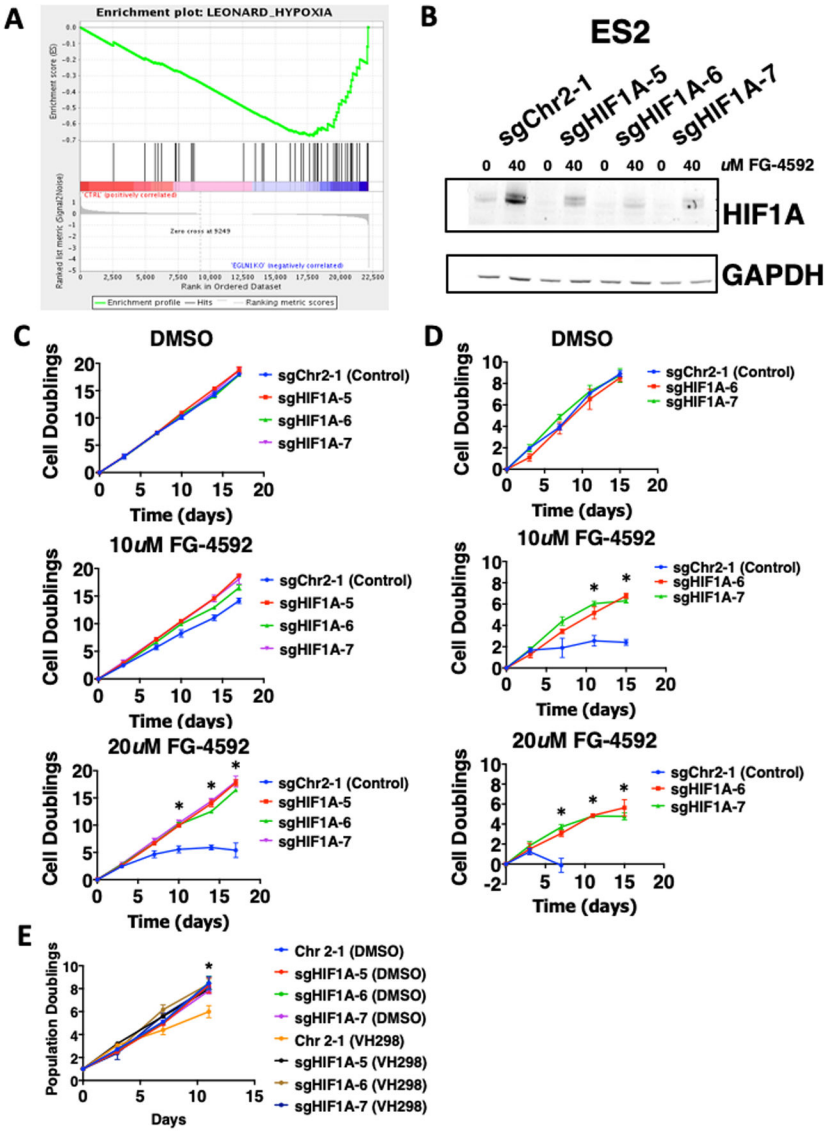

Figure 5. Depletion of HIF1A rescues cells from EGLN1-dependency.

A. RNA sequencing performed on ES2 and OVISE wild-type cells compared to ES2 and OVISE EGLN1 knockout cells. Gene Set Enrichment Analysis of RNA sequencing data shows that HIF1A-related pathways are affected in EGLN1 KO cells.

B. Immunoblot showing efficiency of control sgRNAs (sgChr2–1) or HIF1A deletion with sgRNAs (sgHIF1A-5, sgHIF1A-6, sgHIF1A-7) 48 hours post treatment with control (DMSO) or EGLN1 inhibitor (FG-4592).

C. EGLN1-dependent ES2 cells are resistant to EGLN1 inhibition after HIF1A knockout. DMSO treatment (top) has no effect on control or HIF1A-knockout cells. Increasing treatment with FG-4592 (10 uM middle, 20 uM bottom) reduces proliferation of control cells (blue) but not HIF1A-knock. Results are representative of 3 independent experiments and data is graphed as mean ± standard deviation of 3 replicates. *p<0.05

D. EGLN1-dependent OVISE cells are resistant to EGLN1 inhibition after HIF1A knockout. Similar to ES2 cells, DMSO treatment (top) has no effect on control or HIF1A-knockout

cells. Increasing treatment with FG-4592 (10uM middle, 20uM bottom) reduces proliferation of control cells (blue). Results are representative of 2 independent experiments and data is graphed as mean ± standard deviation of biological triplicates. *p<0.05

E. EGLN1-dependent ES2 cells are resistant to VHL1 inhibition after HIF1A knockout. Treatment with 100uM of VH298 significantly reduces proliferation of control cells (orange) compared to HIF1A knockout cells. Results are representative of 2 independent experiments and data is graphed as mean ± standard deviation of biological triplicates. *p<0.05

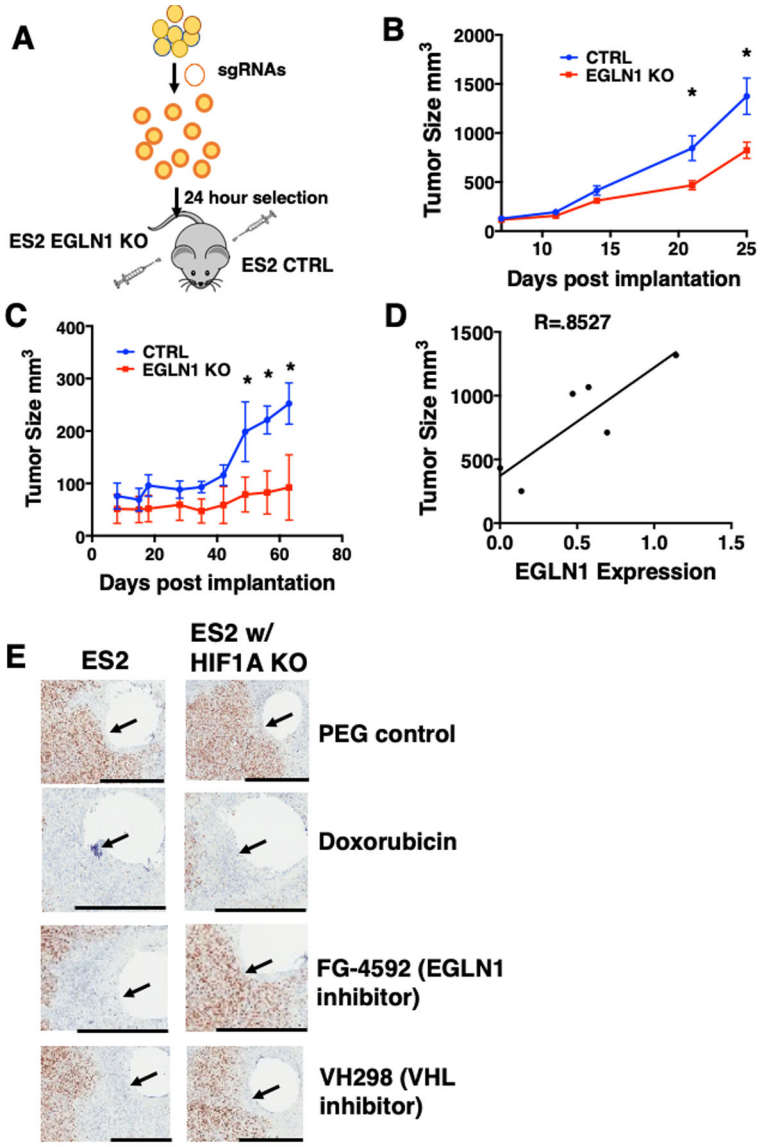

Figure 6. EGLN1 deletion or inhibition reduces tumor formation induced by EGLN1-dependent cells.

A. Schematic of tumor formation experiments. Each recipient mouse receives control (sgChr2–1) and EGLN1-KO cells.

B. EGLN1 knockout impairs tumor formation induced by ES2 cells. Control and EGLN1 KO ES2 cells (100,000) were injected subcutaneously in parallel flanks and tumor size was measured. Data is represented as mean ± standard deviation (n=15) and represents two experimental repeats *p<0.01.

C. EGLN1 knockout impairs tumor formation induced by OVISE cells. Control and EGLN1 KO OVISE cells (250,000) were injected subcutaneously in parallel flanks and tumor size was measured. Data is represented as mean ± standard deviation (n=6) *p<0.05.

D. EGLN1 expression levels in the knockout cells correlate with tumor size. RNA was harvested from tumors and expression was quantified using qRT-PCR. Data is represented as the average of four biological replicates and represents two experimental repeats.

E. Microdevice delivery of EGLN1 inhibitors and VHL inhibitors to ovarian tumor with HIF1A expression reduces proliferation. Microdevices were loaded with PEG-formulated compounds and implanted into $1cm^2$ tumors formed from ES2 or from ES2 with HIF1A KO and grown to $1cm^2$. At 48 hours post microdevice implantation tumors are harvested and serially sectioned and stained. The control for drug formulation (PEG Control) has no effect on the proliferation of ES2 tumor cells with or without HIF1A (top). Doxorubicin treatment reduces tumor cell proliferation (top middle). Inhibition of EGLN1 with FG-4592 blocks proliferation of tumor cells, while knockout of HIF1A rescues EGLN1 inhibition (bottom middle). Inhibition of VHL with VH298 blocks proliferation of tumor cells while knockout of HIF1A rescues VHL inhibition. Figure is representative of three independent experiments. Arrow shows area where drug is released. Black line indicates 1mM.

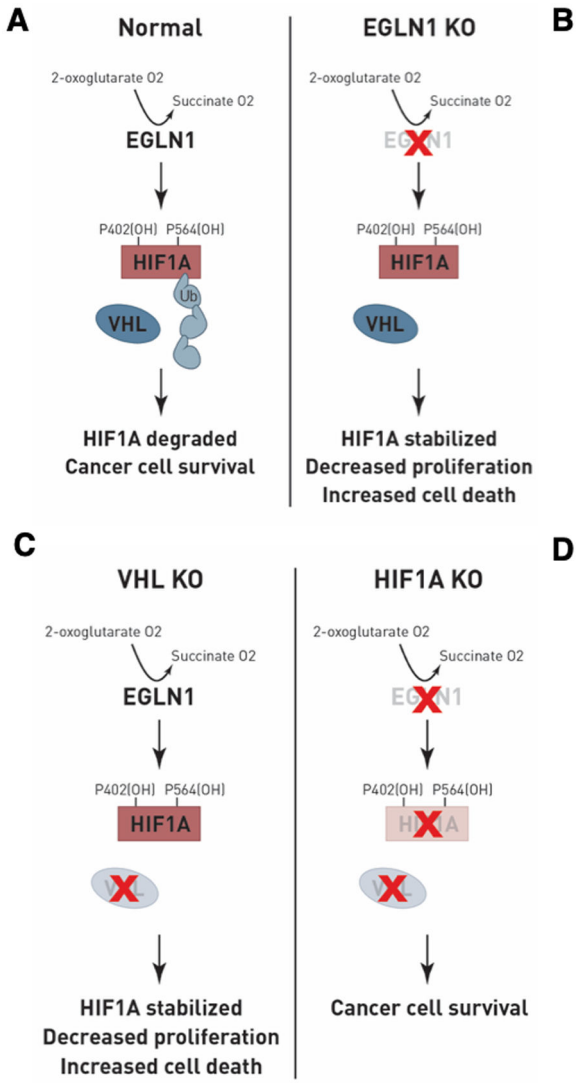

Figure 7. Model of EGLN1 and VHL dependency.

A. Normal conditions. EGLN1 in the presence of oxygen hydroxylates HIF1A at residues P402 and P564. Hydroxylated HIF1A is then targeted for ubiquitination and subsequent degradation by VHL.

B. EGLN1 KO. After EGLN1 KO, HIF1A is non-hydroxylated and therefore not degraded by VHL. Stabilized HIF1A translocates to the nucleus and activates downstream effectors resulting in a decrease in cell viability and increased cell death.

C. VHL KO. Following KO of VHL, HIF1A is hydroxylated by EGLN1 but cannot be ubiquitinated and degraded by VHL. Stabilized HIF1A translocates to the nucleus and activates downstream effectors resulting in a decrease in cell viability and increased cell death.

D. HIF1A KO. HIF1A KO rescues cell proliferation and cell death seen in EGLN1 and VHL KO cells.